EXTERNAL AERODYNAMIC PRESSURE LOADS FOR A RIGID FIGHTER AIRCRAFT, A COMPARISON BETWEEN PSP AND CFD

Pär Gustafsson*, Ingemar Persson*, Neil Stokes**
***SAAB Aeronautics, ****Aircraft Research Association Ltd**
par.gustafsson@Saabgroup.com; ingemar.persson@Saabgroup.com; nstokes@ara.co.uk

Abstract

Comparisons of aerodynamic data obtained from Pressure Sensitive Paint (PSP) measurements and Computational Fluid Dynamics (CFD) analysis are made with balance and pressure taps data. The comparisons are made for both aircraft baseline configurations at a range of angles of attack and for elevator deflection cases at zero degree angle of attack. Both subsonic and supersonic speeds are considered. The PSP test was conducted in the Aircraft Research Association Ltd (ARA) Transonic Wind Tunnel (TWT) in England. The CFD analyses were performed using the EDGE flow solver. The purpose of the PSP test was to generate pressure distributions to be used for aircraft loads analysis, for which CFD also could be used. The comparisons show that both methods compare well with balance and pressure tap data for most cases but diverge for cases where one can expect an aeroelastic influence on the results. In these cases, PSP data is supported by both balance and pressure tap data.

1. General introduction

At SAAB Aeronautics, the concept of unit load cases are emphasized when performing loads analysis on a complete Saab 39 Gripen aircraft. The principle of this concept is that the total set of loads acting on the aircraft for a specified flight condition is a linear combination of unit load cases. One major part of these unit load cases are distributed aerodynamic loads associated with the rigid aircraft. Other unit load cases include dynamic load cases for store separation and landing, internal pressure in fuel tanks, engine attachment loads, pylon attachment loads, cabin pressure, etc.

Since a multirole fighter aircraft such as the Saab 39 Gripen has a quite extensive flight envelope in terms of load factor ($-3 \leq n_z \leq 9$), Mach number (Mach ≤ 2.0) etc., it requires a fairly large amount of unit load cases for the concept of linear combinations of the same to be regarded as valid. It is also important to be able to predict the aircraft life with an as high accuracy as possible and to reduce the structural weight when designing the airframe. In terms of aerodynamic pressure loads this requires the pressure distributions upon which they are based to be as accurate as possible.

Two methods, available today for generation of distributed aerodynamic pressure data are CFD and PSP. This paper will present a comparison between results from these two methods.

2. Background

During the past 25 years, unit load cases for the distributed aerodynamic loads used for loads analysis of the Saab 39 Gripen aircraft have mainly been based on wind tunnel tests where pressure data were generated by pressure taps. When additional data have been required, CFD has been one of the used methods. In recent years, a large PSP test were conducted in the ARA TWT of the complete aircraft, including a wide range of Mach numbers, angles of attack and sideslip as well as model configurations. The aim of the PSP tests was to generate data for a new set of unit load cases, which covers the aircraft envelope in a better way and with a higher accuracy than the old ones. For a few

unit load cases, pressure data for some areas of the aircraft however had to be generated by another method, and also in the future some additional data might be required. For these purposes, CFD is one of the methods that could be used.

3. PSP method and setup

For PSP the model surface is coated with screen layer and paint, and then illuminated with excitation of the appropriate wavelength. The surface is imaged through a long pass filter using a scientific grade CCD camera. The luminescent intensity distribution is recorded and stored for conversion to pressure, using a previously determined calibration. Unfortunately the luminescent intensity distribution is not only a function of the partial pressure of oxygen; in fact the luminescence from the painted surface also varies with illumination intensity, paint layer thickness, and probe distribution. However, if it is assumed that these don't vary in time, they can be eliminated by taking the ratio of the image at the test condition or wind-on image, to an image taken at a known reference condition or wind-off image.

There are two methods for PSP measurement that are most commonly used, Lifetime PSP and Binary PSP. This paper only refers to the Lifetime PSP technique as used in the ARA TWT.

The Lifetime PSP technique is often referred to as the two-gate lifetime PSP method due to the image acquisition process. The paint is excited to fluoresce using a short illumination pulse with data being acquired at two distinct points, Gate 1 and Gate 2, Fig. 1. Gate 1 is acquired simultaneously with illumination and is therefore sensitive to illumination. Gate 2 is acquired after illumination has ceased and is sensitive to both illumination and pressure. By rationing these two gates the sensitivity to illumination is eliminated, leaving the resultant pressure reading. The aim is to optimize the system to obtain a high signal to noise ratio, high pressure sensitivity whilst minimizing the influence of factors such as paint thickness, illumination, and dye concentration.

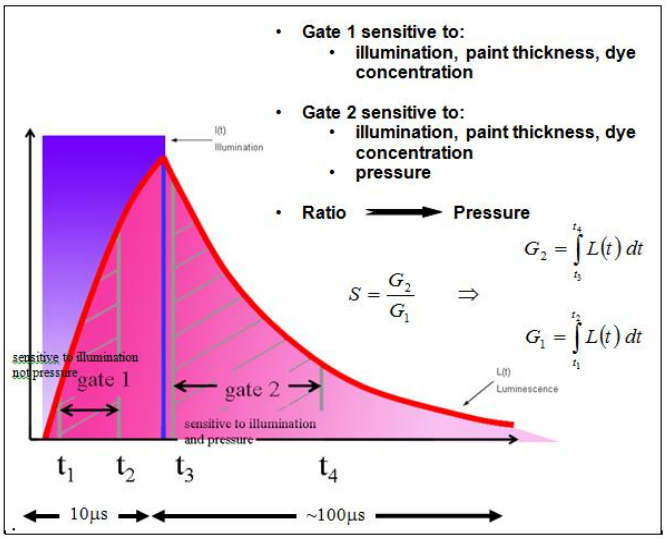

Fig. 1. Two-gate Lifetime PSP

A critical part of the PSP process is determining the intensity versus pressure relationship of the batch of paint being used. When painting the model a sample coupon was also painted. The coupon (of the same material that the model consists of) was then exposed to a series of temperatures and pressures within a calibration chamber and images were acquired. Each intensity acquired was normalized by the intensity at a known reference condition and plotted versus pressure. This highlights one of the issues for concern for PSP measurements, PSP is sensitive to temperature as well as pressure.

During model design and manufacture a small number of marker points were added so that each camera view would have enough reference points to accurately map the images during post-processing. After manufacture, these physical marker points are inspected in x, y, and z co-ordinates, which are then added to the model geometry. From this geometry a mesh was prepared, again for each camera view so that the post-processed images could be mapped accurately onto this mesh and then combined to give the final 3D representation of the pressure distribution across the model surface at any one condition.

Once the model had been assembled and inspected to produce the geometric data required for post-processing it could then be prepared for testing. The first stage was to fully clean the model to de-grease the surface and prepare it for the application of paint. To minimize any temperature variation across different material types, a screen layer was first applied. Once the screen layer had been cured the active PSP layer was applied and cured in a purpose built spray booth and oven. The combined thickness of these two layers was less than 40 μm. Roughness measurements at discrete points across the painted surface were also taken to ensure the smoothest possible application of paint. Once installed into the test facility a paint check was performed to test the response characteristics, evenness of illumination and consistency of acquisition across the multiple camera views.

The equipment used within the ARA Lifetime PSP system is all from the ISSI PSP range of cameras, lamps and software. However, ARA and ISSI have introduced customized modifications to both the hardware and software to improve the productivity and performance of the system and to integrate it into the ARA TWT Data Acquisition System (DAS). The cameras were the PCO 1600MOD bodies with Nikon high performance lenses, the lamps were the ISSI 4" water cooled LED lamps with 12w output in the 450nm UV wavelength. For further details see [1]. For this test there were a total of 12 PSP Cameras and 16 PSP lamps giving the full 3D coverage of the model for all the required test conditions, Fig. 2. All cameras were located in order to get the best possible data quality for as much of the model as possible.

To post process the results, ratios of the wind-on and wind-off images were taken, that eliminates sources of error, illumination, temperature and paint issues. The camera settings and paint calibration were then applied, which gets the pressure values from the paint. This calibrated data was then mapped onto the prepared mesh.

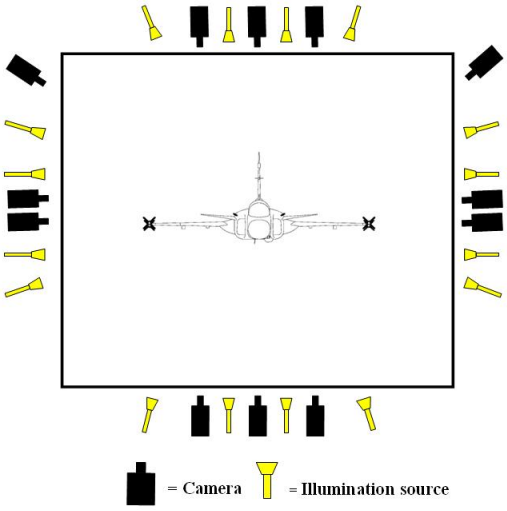

Fig. 2. Schematic of test section

Pressure corrections were performed from the pre-selected pressure tap data for final local temperature compensation.

4. CFD models and computation

A Saab 39 Gripen wind tunnel model has been discretised with and without control surface deflections. The computed models have different levels of modeling complexity in both geometrical realisations as well as flow physical approximations. These are described at greater detail in the following sections.

4.1 Computational Geometry

The CATIA v.4 format geometry files of a Saab 39 Gripen wind tunnel model were prepared at the advanced design office at SAAB. These files were imported into ICEM CFD by using the direct CAD interface add-on module. The models have been modified slightly in order to simplify prismatic grid generation. In particular, some wedge surfaces have been replaced by thin surface strips that are twisted 90 degrees. By doing this, the prism grid generator will produce better cells since the surface normal of adjacent surfaces has a smooth transition while crossing the twisted strip. Furthermore, to terminate the computational domain, a surrounding far field box is placed at distance of approximately 10 characteristic lengths from the aircraft.

4.2 Grid Generation

For this study we have used the ICEM CFD Tetra / Prism grid generator. Tetra creates unstructured tetrahedral grids whereas the prism module creates mixed grids made up of tetrahedral and prismatic elements. The ICEM CFD Tetra software is based upon a modified octree approach. Thus, it generates the whole volume grid directly and the surface grid is simply a restriction of this volume grid to all CAD surfaces. By specifying curves, one enforces the triangle edges to be aligned with these and thereby surface discontinuities are realised. In the same way, by introducing points, one enforces triangle vertices to coincide with these and thus sharp corners are captured. In order to increase the regularity of the surface grid, the surface nodes are then submitted to a few iterations of a discrete version of the Laplacian meanwhile the volume nodes are allowed to float. Since this procedure will destroy the quality of the volume grid, the volume grid is thus smoothed by the regular smoothing procedure whilst keeping the surface mesh nodes frozen. Sometimes, a few smoothing iterations where both the volume nodes and surface nodes are free to move are required to achieve an acceptable quality level. However, only a few iterations are allowed not to destroy the previously achieved regularity. By applying this procedure, a very smooth varying surface mesh, cf. Fig. 3, is kept which is significant in the later process of raising prism layers from the surface. In particular so, as a global height over base control mechanism is applied in the prism generation. The prismatic high aspect ratio elements close to the solid surfaces allow efficient modeling of the high gradients associated with boundary layers. Thus, from this unstructured mesh consisting of tetrahedral volume elements a mixed element mesh is constructed by raising prismatic elements from the surface triangles. The surface normal vectors are smoothed, in order to prevent abrupt changes of the marching direction and crossing of grid lines. The smoothing employed is a weighted Laplacian type where the weighting depends on the surface curvature. The smoothing is applied separately for each layer. An orthogonality control mechanism is relaxed after a few layers. For the viscous computations, a y^+=1 grid holding 43 prismatic layers were used. With an initial prism cell height of $3.2*10^{-5}$ m, the resulting prismatic grid layer expansion factor was approximately 1.2.

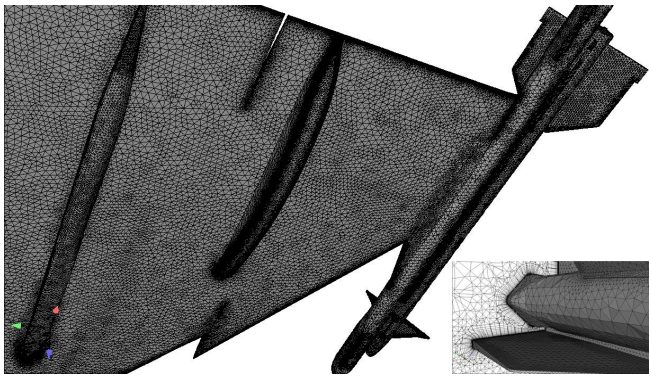

Fig. 3. Surface grid of main wing with inset detail of the volume grid at the missile fins. Note the resolved narrow gaps in between the wing tip pylon and the Sidewinder missile.

In Fig. 4, note how the number of prismatic layers are reduced around the thin gap between the two control surfaces. Typical grid sizes for the mixed grids ranged from 22 Mnodes up to 28 Mnodes, where the grids with most grid nodes have curvature better resolved .

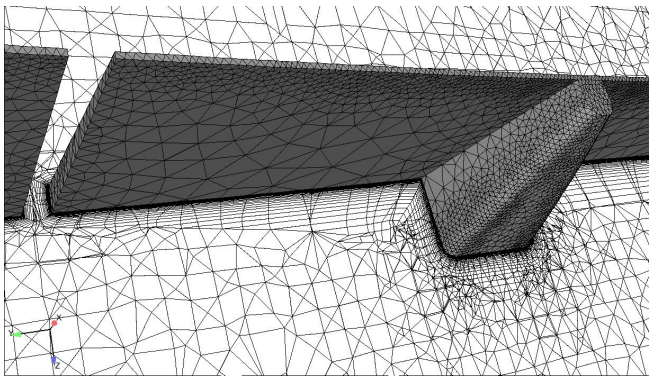

Fig. 4. Straight cut through the volume grid. Note how the prismatic layers are capped down at the control surface gap.

In Fig. 5, the achieved y^+ distribution at supersonic speed is depicted. Only at the very front of the leading edges, y^+ exceeds 1.5.

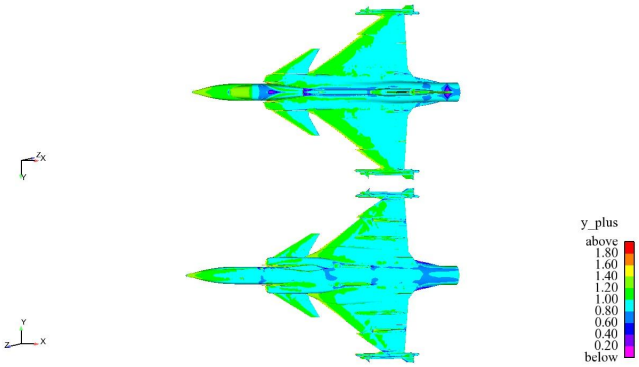

Fig. 5. y^+ distribution at supersonic speed. The common range is $0.8 < y^+ < 1.5$. Only at the leading edges y^+ exceeds 1.5, though below 1.8 on the main wing and below 2 on the canard leading edge.

4.3 Computational Aerodynamics

All the CFD analysis within this study has been conducted with the EDGE (v.5.0) flow solver [2]. The EDGE code is supplied by the Swedish Defense Research Agency (FOI). EDGE is designed to efficiently solve high speed compressible flows. It solves the governing equations on an unstructured hybrid grid which may contain mixtures of tetrahedrons, prisms and hexahedrons. For the solutions presented here, all grids are of mixed prismatic / tetrahedral type. In the study, the code has been used in viscous mode to solve the turbulent full Navier-Stokes equations, i.e. no thin shear layer simplification has been utilised. To model turbulence, the K-ω shear stress transport (SST) model of Menter was adopted. This model includes a shear stress transport relation based on the Bradshaw assumption. Integration in time is carried out by a multi-stage Runge-Kutta scheme with agglomerated full approximation storage multigrid convergence acceleration. All viscous solutions have been initiated by a 1st order upwind scheme and utilising full multigrid (i.e. calculations start on the coarsest mesh) with a 3 grid levels W-cycle strategy in order to quickly establish boundary layers. Thereafter, a central scheme augmented with the famous Jameson-Schmidt-Turkel artificial dissipation has been utilized to establish the final solution. The numerical dissipation has to be added for stabilisation. Boundary conditions are imposed on the far field using Riemann invariants. On solid surfaces, no-slip conditions are enforced. The engine inlet is modeled by a flow through surface just up-stream of the compressor disc. For simplicity, the environmental climate system (ECS) intakes located in the space between the boundary layer splitter plate and the fuselage are realised as a flow through duct.

4.4 Grid refinement

In an attempt to analyze the grid resolution influence, the baseline configuration was computed with two levels of refinement. A fundamental goal is of course to obtain a grid converged solution, i.e. the solution does not change within a certain tolerance with further grid refinement. Such a grid convergence study should always be conducted but given the time it usually takes, this is seldom the case. The grid refinement was done such that emphasis was put on further resolving the curvature on the wing and canard leading edges. The decision to perform a selective refinement was based on the assumption that the wing and canard leading edges are particularly sensitive regions where turbulence production shapes vortex structures that dictate the flow field at large over the delta wing. Furthermore, the main wing fairing was also better resolved on the finest grid. From the achieved integrated results, it was clearly seen that results generally improved on the finer grids. In the discussion and plots below, all results from the first refined grid are omitted as they are intermediate in nature, i.e. in between the original grid and the second refinement.

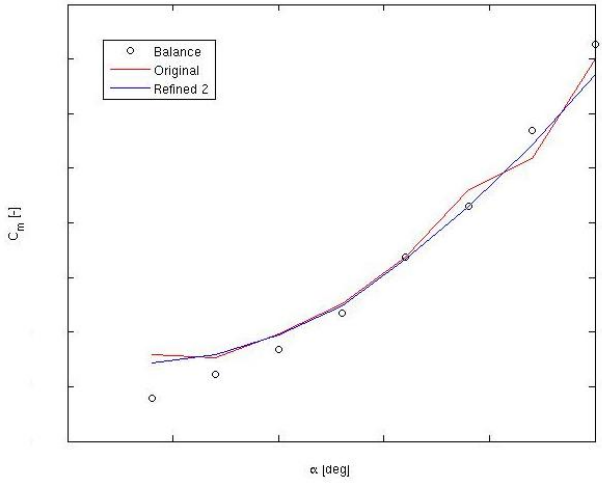

Fig. 6. Computed pitching moment coefficient vs. AoA on the original and the refined grid at subsonic speed.

For the subsonic case, pitching moment improved for all but the highest angle of attack, cf. Fig. 6. The corresponding normal force remained unchanged in the linear region but at the higher angles of attack, the non-linear behavior predicted on the original grid was smoothed out and a better agreement was achieved.

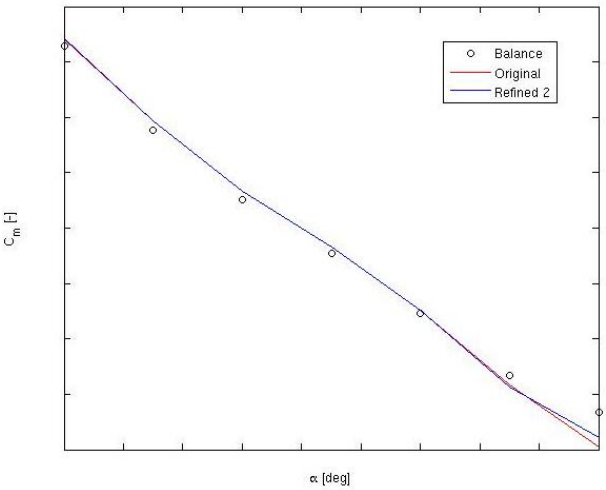

Fig. 7. Computed pitching moment coefficient vs. AoA on the original and the refined grid at supersonic speed.

Thus, it is an example of the delicate task to get the pressures correctly predicted around the reference point. At this high angle of attack we have that due to the performed grid refinement the computations not only generates a stronger inner wing vortex but also the distance until vortex break-down is longer. Thus affecting a large part of the upper wing side downstream of the reference point with a negative pressure coefficient. Adding to this increased differential nose-down moment is also the effect of a secondary vortex generated outboard of the main wing saw-tooth. These conditions are not counter balanced by the canards, nor by the inner wing vortex upstream of the reference point. At the low transonic condition, examining differences at low to medium negative angles of attack, no significant difference could be seen for the normal force. Regarding pitch, the original grid gave in fact the best results. For the supersonic case negligible differences could be seen in the normal force. The same applies to the pitching moment for all but the highest angle of attack, where the refined grid improved the results, cf. Fig. 7. Nevertheless, the predicted pitching moment for this angle of attack still is in poor agreement with the experimental data. For each speed regime, comparisons with pressure tap data have been conducted. Primarily for medium negative angles of attack, as the number of taps available for comparisons are much larger on the main wing lower side where they also are quite well distributed over the wing area. However, upon examination of the specific positions with pressure taps, it was not obvious how to conclude. One key problem being that no pressure taps exist at the increasingly resolved area. To conclude, the performed study showed that we have not established grid independence. Although the refined grids generally improve results, there are also a few conditions where the opposite hold. More refinements would be needed to gain further insight. However, from this study, an insight is that surface element sizes commonly used on the leading edges are too large.

4.5 Turbulence model variation

Apart from the grid refinement study, a variation of the used turbulence models was also conducted. Here, the standard Menter SST k-ω model was replaced by either the Wallin & Johansson EARSM with Hellsten k-ω or the Wallin & Johansson Curvature Corrected - EARSM with Hellsten k-ω. Upon inspection of the results for a moderate negative angle of attack at low transonic speed, it was concluded that the changes seen are deemed to be of subordinate importance.

5. Results

Flow conditions used in the comparisons are restricted to pure subsonic and pure supersonic, due to confidentiality reasons. Aircraft configurations used are baseline e.g. no control surface deflections at a range of angles of attack and zero degree sideslip, both positive and negative elevator/aileron deflections of the same magnitude i.e. δ_E at zero degree angle of attack and sideslip.

CFD data presented in this section for comparisons with PSP-, balance- and pressure taps-data are based on the original grid quality as described in section 4. Flow physical parameters such as Reynold's number, dynamic pressure etc are comparable to wind tunnel conditions.

Presented results include comparisons of pure pressure coefficient data, i.e. Cp-values generated by PSP, CFD and pressure taps, where the pressure tap data refers to pressure taps located on the port wing lower side, schematically illustrated in Fig. 8, labeled as Y1-Y4. These pressure taps have not been used for correction of PSP-data.

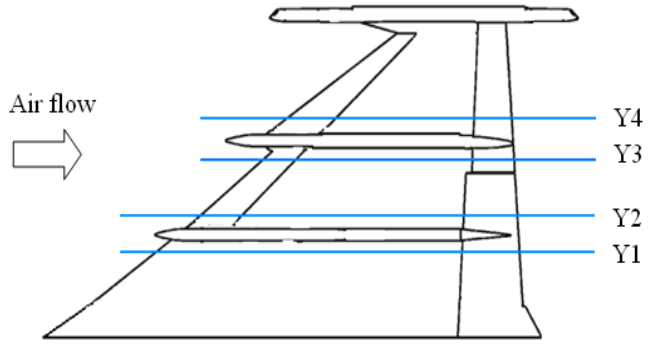

Fig. 8. Location of pressure taps sections Y1-Y4 on left main wing lower side.

Comparisons are also made on the overall aerodynamic loads for the complete aircraft and for the port side canard wing. For the complete aircraft, balance data from the wind tunnel test are included. No PSP-data were captured on the wingtip pylons or missiles, due to the complex surfaces. To account for that in the comparison with balance and CFD data, results from the CFD calculations for these features are added to the PSP results. For the complete aircraft, normal force (C_N) and pitching moment (C_m) are considered only (symmetric configurations). For the port canard wing, all three components, normal force (C_{Nnv}), bending moment (C_{bnv}) and hinge moment (C_{hnv}) are considered. For elevators and ailerons, only the hinge moments C_{he} and C_{ha} are considered.

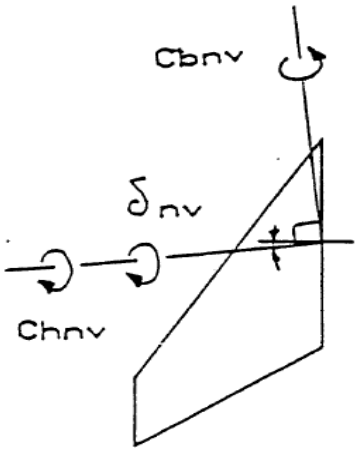

Fig. 9. Port canard wing moment definitions.

5.1 Angle of attack cases

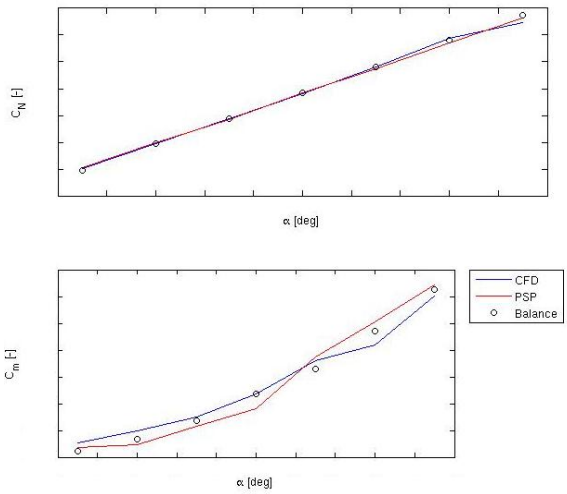

Fig. 10. Aircraft loads C_N and C_m at subsonic speed.

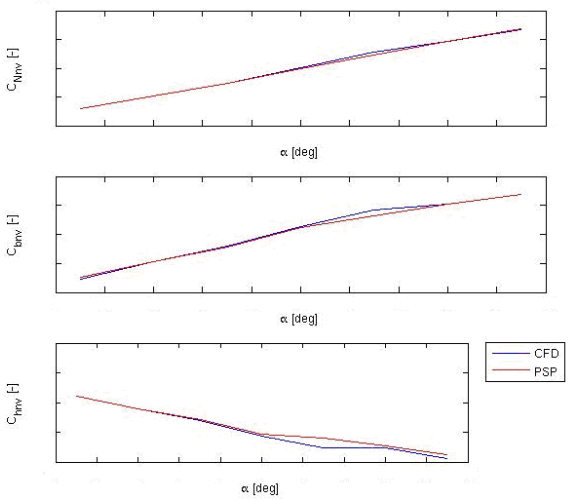

Fig. 11. Port canard wing loads, C_{Nnv}, C_{bnv} and C_{hnv} at subsonic speed.

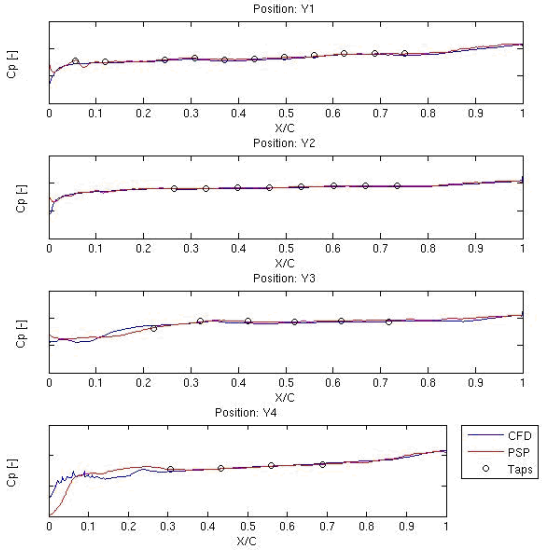

Fig. 12. Cp at subsonic speed and low angle of attack.

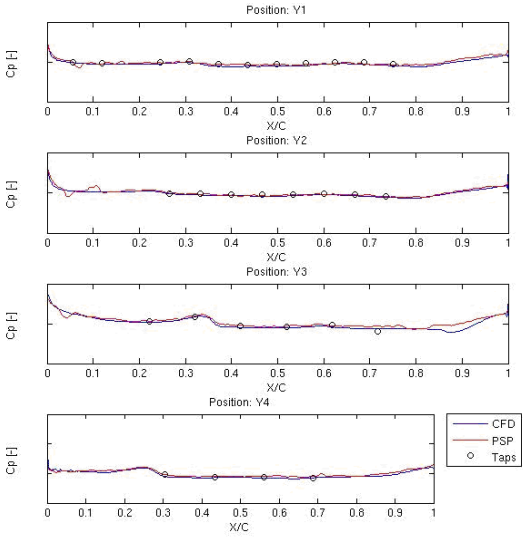

Fig. 13. Cp at subsonic speed and medium angle of attack.

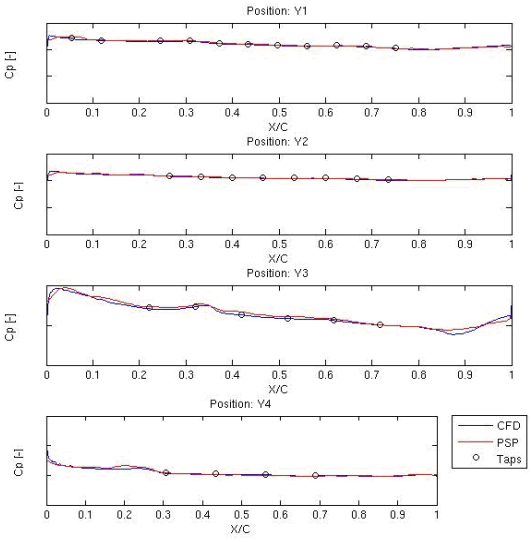

Fig. 14. Cp at subsonic speed and high angle of attack.

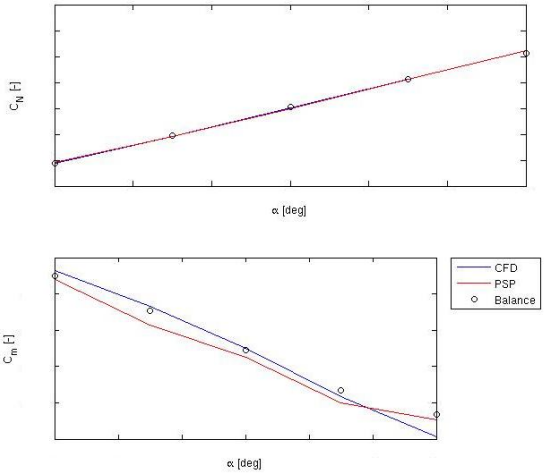

Fig. 15. Aircraft loads C_N and C_m at supersonic speed.

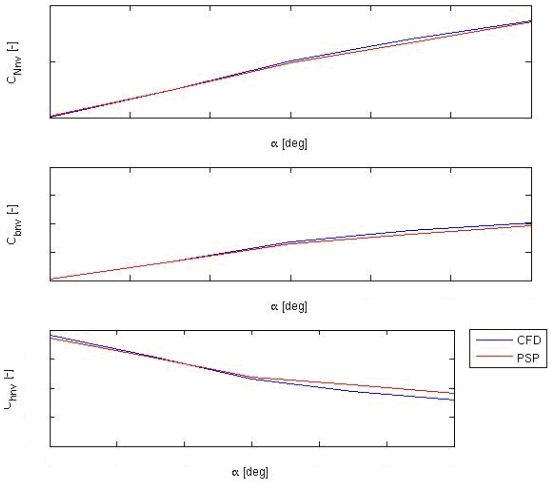

Fig. 16. Port canard wing loads C_{Nnv}, C_{bnv} and C_{hnv} at supersonic speed.

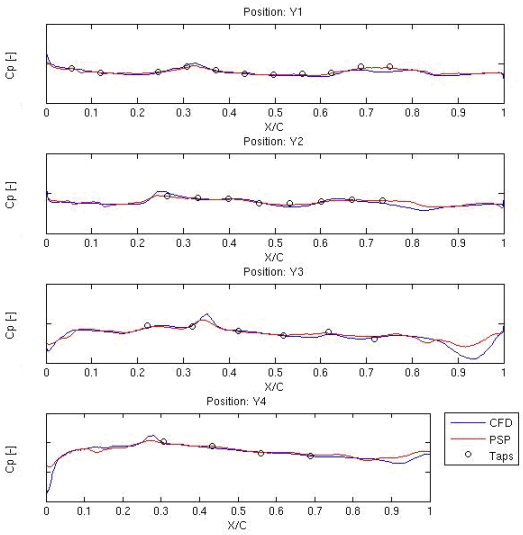

Fig. 17. Cp at supersonic speed and low angle of attack.

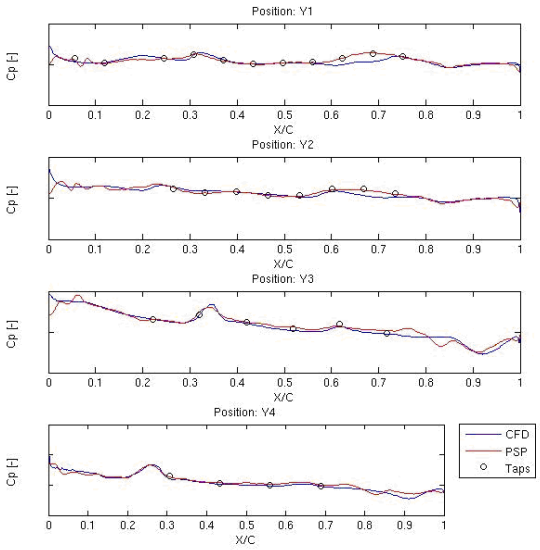

Fig. 18. Cp at supersonic speed and medium angle of attack.

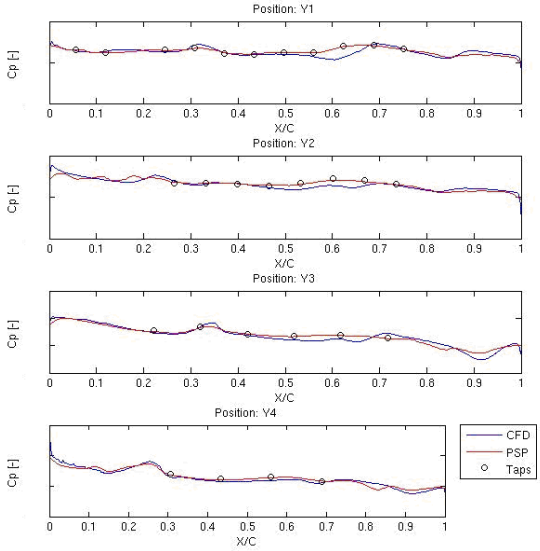

Fig. 19. Cp at supersonic speed and high angle of attack.

Both methods, CFD and PSP show good match with balance data for the complete model. For the normal force C_N, both methods show an almost exact match for both subsonic and supersonic flow regimes. The pitching moment C_m is in general equally well captured by both methods, where the PSP results show an overall slightly better match at subsonic speed than the CFD results. Reversely, at supersonic speed, the CFD results show an overall better match than the PSP results. For the port canard wing loads, the CFD and PSP results compare well, especially for low angle of attack. For the subsonic case, the loads diverge at medium angle of attack, in order to match very well again at high angle of attack. For the supersonic case, the match is very good for low angle of attack but diverge slightly for high angle of attack, this is most evident for the hinge moment C_{hnv}. For the main part of the wing at subsonic speed, the pressure coefficient C_P generated by both CFD and PSP show a good match with pressure taps data. The methods diverge somewhat close to the leading edge and also at $x/c > 0.85$ for position Y3 and Y4, cf. Figs. 12-14. For supersonic speed, PSP shows a better match with pressure taps than CFD as depicted in Figs. 17-19. However, flow features at $0.25 < x/c < 0.4$ for positions Y3-Y4 are captured quite well by both methods, which also is proven by pressure taps as most clearly depicted in Fig. 18.

5.2 Elevator-aileron deflection cases

δ_E	Balance		PSP		CFD	
	ΔC_N	ΔC_m	ΔC_N	ΔC_m	ΔC_N	ΔC_m
-	-0.2206	0.0940	-0.2280	0.0926	-0.2429	0.1071
+	0.2005	-0.0928	0.1867	-0.0845	0.2426	-0.1070

Table 1. Aircraft delta loads ΔC_N and ΔC_m due to δ_E at subsonic speed.

δ_E	PSP		CFD	
	ΔC_{he}	ΔC_{ha}	ΔC_{he}	ΔC_{ha}
-	0.1156	0.1303	0.1179	0.1193
+	-0.0923	-0.1005	-0.1205	-0.1187

Table 2. Elevator/aileron delta hinge moments ΔC_{he} and ΔC_{ha} due to δ_E at subsonic speed.

δ_E	Balance		PSP		CFD	
	ΔC_N	ΔC_m	ΔC_N	ΔC_m	ΔC_N	ΔC_m
-	-0.1009	0.0692	-0.1006	0.0634	-0.1147	0.0785
+	0.0907	-0.0672	0.0839	-0.0599	0.1097	-0.0755

Table 3. Aircraft delta loads ΔC_N and ΔC_m due to δ_E at supersonic speed.

δ_E	PSP		CFD	
	ΔC_{he}	ΔC_{ha}	ΔC_{he}	ΔC_{ha}
-	0.2333	0.2337	0.3327	0.3442
+	-0.2496	-0.2695	-0.3359	-0.3574

Table 4. Elevator/aileron delta hinge moments ΔC_{he} and ΔC_{ha} due to δ_E at supersonic speed.

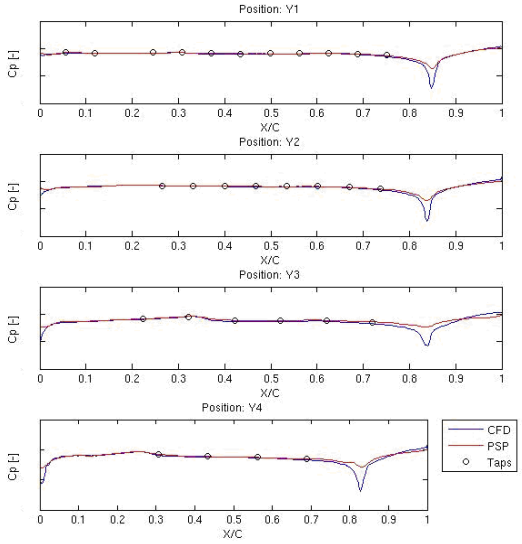

Fig. 20. Cp at subsonic speed and negative δ_E.

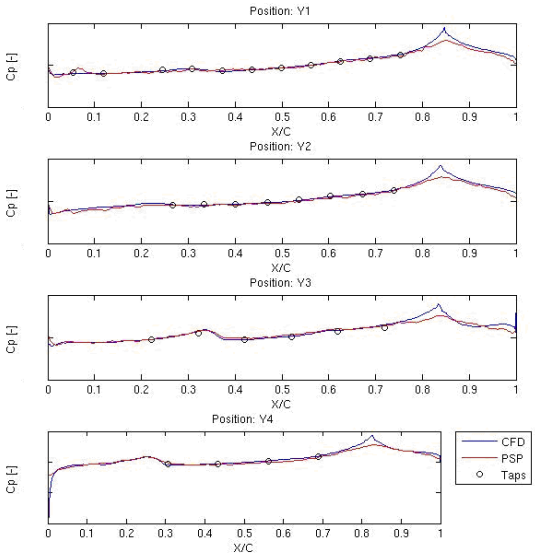

Fig. 21. Cp at subsonic speed and positive δ_E.

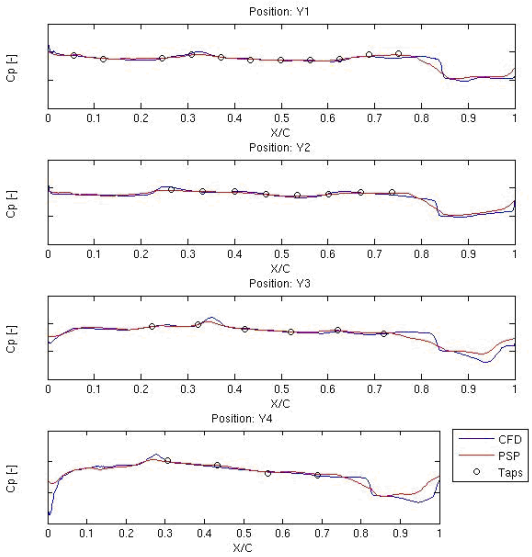

Fig. 22. Cp at supersonic speed and negative δ_E.

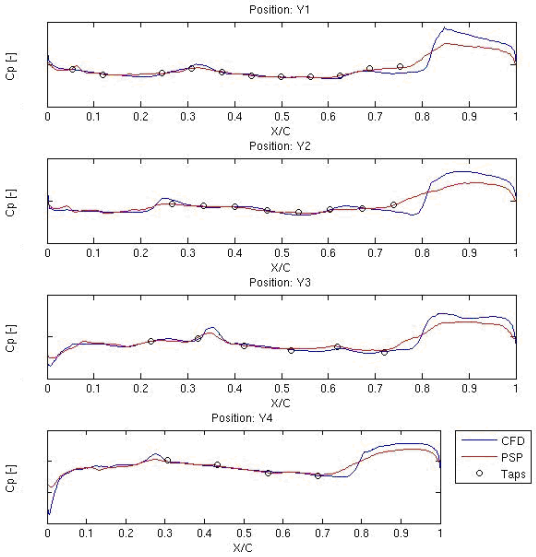

Fig. 23. Cp at supersonic speed and positive δ_E.

The aerodynamic coefficients data presented in this section are delta effects due to δ_E control surface deflection at zero degree angle of attack and sideslip. As can be seen in Table 1 - Table 4, PSP shows a better match with balance data for the complete aircraft than CFD, especially in the supersonic flow regime. In general, CFD shows larger delta effects than PSP. Regarding the elevator and aileron hinge moments, C_{he} and C_{ha}, CFD predicts a higher delta effect with one exception, negative δ_E at subsonic speed. For the supersonic flow regime, the CFD predicted ΔC_{he} and ΔC_{ha} are about 50% higher than the ones predicted by PSP.

The differences presented for hinge moments are also supported by the pressure coefficients comparisons with pressure taps data in Figs. 20-23, where a good match with pressure tap data is given by both methods for the main part of the wing ($0.05 < x/c < 0.75$) in both subsonic and supersonic flow regimes. In subsonic speed, the CFD and PSP results mainly diverge from each other close to the elevator and aileron hinge lines, where PSP show a much smoother pressure gradient across the hinge line than CFD in order to compare quite well again as x/c increases. In the supersonic flow regime, the mentioned differences at subsonic speed become even more noticeable and as x/c increases, the results from the two methods still do not compare very well.

6. Conclusions

As shown and mentioned, in general both methods compare quite well with both balance and pressure tap data. Where they diverge from each other regarding comparisons with pressure taps, the PSP results are supported by the pressure taps.

Repeatable differences associated with the main wing leading edge is mainly thought to be a result of the geometric curvature of a leading edge for which no PSP camera location was optimized. The number of cameras was limited to 12 and other areas on the model had higher priority. The slightly too high y^+-values primarily influence the shear stresses associated with the boundary layer. Its influence on the predicted pressure distributions is small and will only have a minor influence on the predicted aircraft aerodynamic loads. As a consequence of this, the CFD results is regarded as the most trustworthy ones closest to the leading edge of the main wings for the general case, even though the y^+-values in these areas are slightly too high.

For angle of attack cases i.e. section 5.1, differences at $x/c > 0.85$ for Y3 and Y4 are associated with the gradual expansion of the flow generated by the curvature of the hydraulic casing. CFD predicts a stronger expansion than is shown by PSP. Position Y3 is located closer to the hydraulic casing than position Y4 and also on the inner side of the casing where the expansion of the flow is stronger than on the outer side, thus position Y3 shows the largest difference.

The geometry at the elevator and aileron hinge lines for the δ_E cases i.e. the geometrical curvature across the hinge lines varies for the discrete CFD model as compared to the PSP painted wind tunnel model. The actual curvature is not resolved in the discrete CFD model, but is represented as a sharp edge. The effect of a more accurately resolved curvature has been studied, resulting in only minor adjustments as compared to PSP data, this by resolving it by about 3 surface elements in the direction of the flow. As for the hydraulic casing it is shown that the CFD predicts a stronger expansion of the flow due to geometrical curvature across the hinge lines for the negative δ_E cases than is shown by PSP. For the positive δ_E cases, CFD predicts a stronger compression of the flow than is shown by PSP. The effect on the geometrical curvature across the hinge lines by applying primer / paint and its influence on the flow field is believed to be negligible. This since the total screen layer and paint thickness was less than 40μm, and the results by studying a resolved curvature across the hinge lines compared to a sharp edge by CFD, only resulted in minor adjustments.

The presented results for which the two methods diverge the most, loads on the elevator and aileron for the δ_E cases, at supersonic speed and zero degree angle of attack and sideslip, aeroelastic effects on the wind tunnel model is believed to be a part of the explanation. This since the comparisons show good match for baseline configurations as a function of angle of attack and also a fairly good match for δ_E cases at subsonic speed, where the dynamic pressure is low compared to the supersonic case. In general it is common practice to assume a fighter aircraft wind tunnel model like the one used to behave in a rigid manner, which strictly speaking of course is wrong. Aeroelastic deformation of the wind tunnel model will influence both CFD and PSP results when compared to balance data and/or pressure tap data. The CFD do not take aeroelastic deformation into account and regarding PSP, model deformation will have an impact on the results due to the ratios of wind-on and wind-off images, which are evaluated in order to eliminate sources of errors. In short words, in case of model deformation, the wind-on and wind-off images are not acquired for the same geometry or more important the same illumination intensity for all model surfaces, which will influence the quality of the PSP results, for further details see [1]. The aeroelastic effects on the wind tunnel model used is today unfortunately unknown.

As PSP data is supported especially by pressure taps but also balance data in a slightly better way than the CFD data, PSP is believed to be the better choice of method for generating the main part of the aerodynamic unit load cases. This by also taking into account the computational cost in terms of time, required to generate the very large number of well resolved and converged CFD data for all model configurations. Using PSP for the purpose can also provide both balance data and pressure taps data, which can and should be used for data quality checks, which is highly valuable. It should though be kept in mind that what is meant to be a specified test condition in the wind tunnel might not be true due to aeroelastic effects. The comparison however also show that CFD can be used, especially for filling gaps where PSP data could not be generated for some reason and also for generating a complete unit load case which needs to be added to the database of unit load cases later on. However the areas of the aircraft and the flow condition for which CFD data are being used should be thought through carefully, based on differences presented in this paper.

7. Future work

To gain an even better understanding of how the two methods compare and how accurately they capture the actual distributed aerodynamic loads, balance data for individual control surfaces or individual lifting surfaces such as wings or canard wings, would be of significant importance. Also the aeroelastic behavior of the wind tunnel model subjected to wind tunnel test conditions and how it influences the results should be studied.

8. Acknowledgement

The authors would like to thank the ARA PSP team for their support and contribution in completing the PSP test. Likewise regarding geometry creation, the authors would like to thank mr Ronny Gyllensten and mr Håkan Roback for their excellent CAD work. Special thanks also to SAAB Aeronautics loads department technical fellow, mr Bengt Mexnell, who has been involved in the Saab 39 Gripen PSP test campaign from initiation of the idea using PSP as a method for our application, to the final evaluation of the obtained data.

References

[1] Vardaki E., Stokes N., Patel S., Gustafsson P., Pressure sensitive paint measurements on the gripen model at the ARA transonic wind tunnel. *50th AIAA Aerospace Science Meeting*. Nashville, Tennessee. AIAA-2012-1188. 2012.

[2] Eliasson P., EDGE, a Navier-Stokes solver for unstructured grids. Proc. To Finite Volumes for Complex Applications III, pp 527-534, 2002.

Copyright Statement